Quality assessment of Airborne Image Spectrometry Data for the AVIRIS-4

Laurent V. Jospin, Jesse Lahaye, Jan Skaloud

Environmental Sensing Observatory (ESO), Ecole Polytechnique Fédérale de Lausanne (EPFL), Lausanne, Switzerland – (laurent.jospin, jesse.lahaye, jan.skaloud)@epfl.ch

Keywords: Airborne Imaging Spectrometry, Photogrammetry, Open Data, Dynamic network

Abstract

The AVIRIS-4 is a state of the art imaging spectrometer developed by NASA-JPL for the consortium of Swiss universities ARES. Measurement campaigns using this instrument started in 2024. According to the agreement with NASA-JPL, all imagery produced by the AVIRIS-4 should be made available as open data. To support the efforts of the ARES consortium in improving the quality and interoperability of the produced research data, in line with the FAIR framework for open data, a new tool is proposed to label tie points on hyperspectral imagery and use them as quality control indicators of the georeferencing process. A case study on the first flight of the system acquired for the geometric calibration of AVIRIS-4 is presented. Based on the proposed quality indicators, errors in the measured trajectory data collected in flight were identified, indicating the need for a new calibration flight, further refinement of the proposed trajectory optimization framework and guiding the design of future missions.

1. Introduction

The AVIRIS-4 imaging spectrometer, is a state of the art sensor developed by NASA-JPL in 2022 and entered service in Europe in 2024 by the Swiss-university research consortium, the Airborne Research Facility for the Earth System (ARES) (Hueni et al., 2025). During its lifetime, a tremendous volume of high-resolution airborne imaging spectrometer (AIS) data will be produced along with raw navigation data. According to the agreement with NASA-JPL, all AVIRIS-4 data collected must be published as open access. To maximize the impact when sharing these research data publicly, the consortium strives to apply the guidelines and practices of the FAIR (Findable, Accessible, Interoperable and Reusable) principles (Wilkinson et al., 2016, Jacobsen et al., 2020).

End-users of the AVIRIS-4 data include specialists in computer vision and/or navigation, who are interested in creating tools and methods to improve sensor fusion or photogrammetry algorithms and need ground truth references for testing purposes; as well as remote sensing and environmental scientists who want to extract information from the final data for different practical applications, e.g., vegetation monitoring (Behmann et al., 2014), snow cover analysis (Varade et al., 2017) or methane detection (Kumar et al., 2020). The latter group requires the AIS data to have a certain quality, knowledge of the estimated georeferencing accuracy for purposes of combining it with other data sources (e.g. field measurements, airborne/satellite data, etc.) and additional metadata to ensure interoperability and re-usability of the AVIRIS-4 data, see Figure 1. In addition to the line spectrometer producing raw push-broom sequences, the inertial navigation system embedding a high-end GNSS receiver is attached to the camera to measure information on the trajectory that is employed for real-time platform stabilization, and in post-processing to estimate a flight trajectory of the acquired AIS data for purposes of direct georeferencing. The later stages involves differential GNSS processing using data from ground receivers and is conventionally performed by Kalman Filtering followed by recursive smoothing to produce a Smooth Best Estimate of Trajectory (SBET). With the knowledge of AIS interior orientation and system mounting, the raw AIS images can be combined with the SBET to produce ortho-images. Quality indicators such as the variance of the raw data (GPS/INS + AIS) are important for the interoperability and re-usability (per FAIR principles), of both raw imagery, GNSS/INS data, the resulting SBET as well as final ortho-image. Therefore, quality assurance (QA) measures need to be put in place to ensure that collected and produced data and metadata is sufficiently correct before being distributed as analysis ready data (ARD).

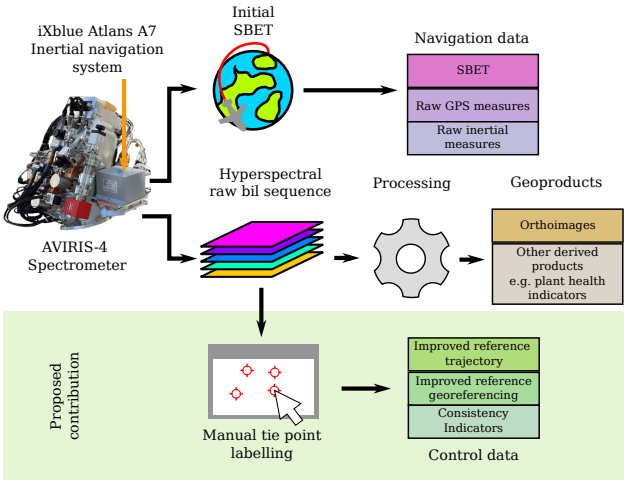

Figure 1. Data and metadata produced by the AVIRIS-4

As part of the Swiss ETH-Domain open research data (ORD) initiative, we have developed an open software, called MAnual-LAbeling for HYperspectral Data (MALAHYD), to assist in producing independently controlled metadata for AIS images. The tool is built as an interface to label image correspondences (tie points) between AIS images and/or corresponding data-sources such as digital surface models (DSM) or digital terrain models (DTM). Manual tie points offer an important complement for AIS data as:

- An effective tool for QA of the refined navigation and georectification solutions. This is a useful feature to have

in general, but is especially important for push-broom images, including AIS data, as the quality of the image rectification depends more heavily on the trajectory quality as compared to frame images.

- As an independent ground truth for developing and evaluating novel georeferencing algorithms. Alternatively, tie-points can be used with existing algorithms for georeferencing to improve the precision and accuracy of the reference solution, which, in turn, can be used as a baseline for comparison.

This contribution presents, in Section 2, the technical details and design of the user interface of the MALAHYD tool. Section 3 discusses how manual tie points can be used for QA or as a (pseudo) ground truth. As a practical example of the MALAHYD application, Section 4 details the initial analysis of the first data produced by the AVIRIS-4. Section 5 concludes this work by giving some perspective on MALAHYD and how it will support the efforts of the open research data efforts of the ARES consortium.

2. The MALAHYD and related tools

MALAHYD is developed as part of an extension module [1] for the SteviApp photogrammetry software [2], initially conceived by the first author during his Ph.D thesis (Jospin, 2023).

2.1 Functionality

MALAHYD enables users to load AIS images in the ENVI BIL standard file format on which they can identify and manually label landmarks, as shown in Figure 2. A common landmark marked on at least two images represents a tie-point. Landmarks established on one image are indexed as 'Active landmarks' within the software so that they can be easily tracked and attributed to following images (see Figure 2 upper right corner of window).
The software also enables users to label landmarks on digital elevation models (DEM), DSM for surface or DTM for terrain. Labels marked between the DEM and AIS images as tie-points serve to provide a measure of the geometric consistency between the raw AIS imagery and the digital terrain or surface models which is important to ensure the quality of the final orthoimage products. In that sense, tie-points between AIS images and DEM act as "pseudo" ground control points which are useful as constraints in the optimization and rectification of the Navigation and AIS data and for QA of the distributed data products. Tie-points identified on DSM are favored over comparisons with orthoimages and other 2D sources. This is not only because the 3D points offer more information, but also to avoid parallax effects on orthoimages which were produced using a DTM rather than a DSM. DSM are also important for the further processing of AIS images, making tie points with a DSM an important control feature. In addition, a generic file exchange format has been created to import/export a broad set of tie-point formats for use between other tools (e.g. correspondences with orthoimages, as used in some hyperspectral processing tools such as PARGE (Schläpfer and Richter, 2002)).

[1] Available at `https://github.com/french-paragon/PikaLTools/tree/main/tools/MalahydSteviappModule`
[2] Available at `https://github.com/french-paragon/steviapp`

2.2 Parameter sets and external data

Within the software, images can be linked to a trajectory data-block, the geometrical parameters of push-broom camera and the system mounting parameters (data-block) encompassing the boresight and lever arm. Unlike frame imagery, where it is sometimes possible to derive a DSM from a point cloud constructed from the images themselves (using Structure from Motion - SfM), and then use point-cloud resulting DSM for image ortho-rectification, it is preferable to use external DSM for that purpose in AVIRIS-4. This can be either a specific lidar point cloud or a national-wide DSM/DTM. This is because, with a single-line, push-broom sensor like AVIRIS-4, the poses are different for each image-line and as such, it becomes much more complex to produce dense point clouds using SfM.

2.3 Camera intrinsics

Steviapp implements a specific camera model for push-broom pinhole sensors, like the AVIRIS-4. The model is:

$$\begin{bmatrix} u \\ v \\ 1 \end{bmatrix} = \begin{bmatrix} f & 0 & pp_x \\ 0 & f & 0 \\ 0 & 0 & 1 \end{bmatrix} \left(\frac{1}{z_c} \mathbf{\Gamma} \begin{bmatrix} x_w \\ y_w \\ z_w \end{bmatrix} - \begin{bmatrix} \Delta x(u) \\ \Delta y(u) \\ 0 \end{bmatrix} \right), \quad (1)$$

where u is the pixel coordinate on the line, f is the camera constant in pixels, pp_x is the principal point, x_w, y_w, z_w are the point world coordinates, $\mathbf{\Gamma}$ is the pose of the camera, including the 3×3 rotation matrix $\boldsymbol{R}$ and 3D position vector $\boldsymbol{t}$ and $\Delta x(u), \Delta y(u)$ are lens distortion models along- and across-track direction, respectively. The along-track component v of the projected points is assumed to be 0, if it is not, then the position of the camera is not considered at the time the point was visible. Small v can also occur during the optimization process, or indicate a re-projection error in the along track direction.

$\Delta x(u)$ and $\Delta y(u)$ are parametrized as polynomials of degree 5, similar to the model proposed in (Zhang et al., 2018):

$$\begin{aligned} \Delta x(u) &= \sum_{i=0}^{5} a_i \left(\frac{u - w/2}{w} \right)^i, \\ \Delta y(u) &= \sum_{i=0}^{5} b_i \left(\frac{u - w/2}{w} \right)^i, \end{aligned} \quad (2)$$

with u being the pixel coordinate and w the width of the pixel array.

Finally, the camera boresight $\boldsymbol{R}_b^c$ and lever arm t_b^c with respect to the inertial trajectory are also part of the intrinsic parameters related to the camera-IMU system. In the case of the AVIRIS-4, the inertial navigation system is attached to the body of the sensor, so $\boldsymbol{R}_b^c$ and t_b^c should stay time-invariant between missions.

2.4 Optimization

SteviApp uses a factor graph to determine the optimal camera poses and intrinsic parameters, using a method derived from the Dynamic Network model (Cucci et al., 2017). In a large simplification, this can be understood as a set of parameters $\boldsymbol{x}$ to be determined with respect to the collection of related (mostly non-linear) error functions $\boldsymbol{r}(\boldsymbol{x})$. The optimization is the process of finding the optimal values $\hat{\boldsymbol{x}}$ minimizing the sum of the

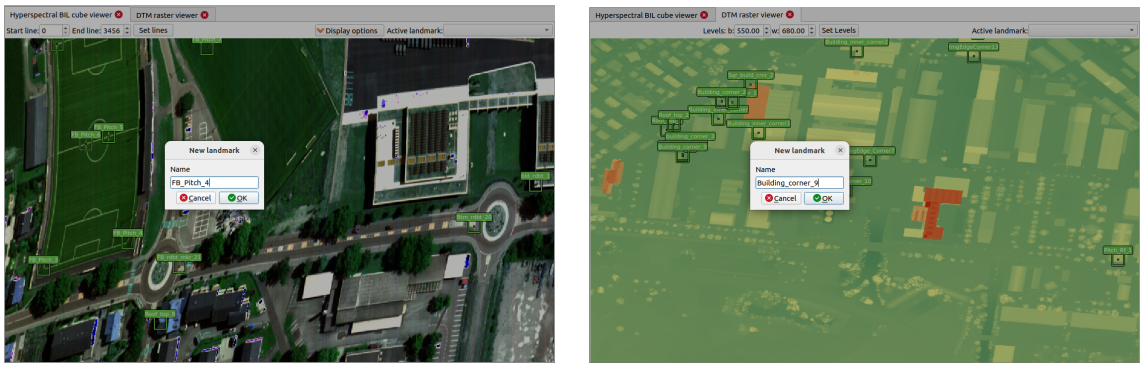

(a) AIS images (b) DSM

Figure 2. Data labeling interface

squares of the error functions $\boldsymbol{r}(\boldsymbol{x})$. Starting from an estimate $\mathring{\boldsymbol{x}}$ close to the optimal solution $\hat{\boldsymbol{x}}$, the system can be linearized. The optimal solution is then given by:

$$\hat{\boldsymbol{x}} = \mathring{\boldsymbol{x}} - \boldsymbol{H}^{-1}\boldsymbol{J}^{\top}\boldsymbol{W}\boldsymbol{r}(\mathring{\boldsymbol{x}}), \tag{3}$$

where $\boldsymbol{H} = \boldsymbol{J}^{\top}\boldsymbol{W}\boldsymbol{J}$ is the Hessian matrix, $\boldsymbol{J}$ is the Jacobian of the system, $\boldsymbol{W}$ is a weight matrix and $\boldsymbol{r}(\boldsymbol{x})$ are the residual functions in the factor graph. $\boldsymbol{W}$ represent the inverse of the a-priori covariance of the residuals.

3. Quality assessment model

Two metrics are important when assessing the quality of the georeferencing of the data: the relative accuracy, which measures the consistency of the data with itself, and the absolute accuracy, which measures the consistency of the data with an independent comparison of a superior quality, e.g. an independently determined coordinates of point(s) in a geodetic spatial reference system (SRS).

3.1 Relative accuracy

We propose three different metrics to assess the relative accuracy of the AVIRIS-4 images: (i) the re-projection error of tie-points, (ii) the a-posteriori uncertainty of the intrinsic parameters and (iii) the relative consistency of the estimated intrinsic parameters (camera and system) either between missions or between separate portions within the same, larger, mission.

The tie-point reprojection error is computed in both the across-track (u) and along-track (v) directions using Equation 1. While the v direction usually represents time, in this case it can still be interpreted as a distance measure, as it corresponds to a misalignment in the angle between the actual (optimized) viewing direction of the camera/line to the estimated tie point position and the expected viewing direction between the camera/line and the point according to the projection model.

In case no optimization has been performed, it is still possible to compute a reprojection error from the set of initial parameters by first computing the estimated point position as:

$$\frac{1}{2}\left([\boldsymbol{v}_0\ \boldsymbol{v}_1]\left(\boldsymbol{V}^{\top}\boldsymbol{V}\right)^{-1}\boldsymbol{V}^{\top}(\boldsymbol{t}_1 - \boldsymbol{t}_0) + \boldsymbol{t}_0 + \boldsymbol{t}_1\right), \tag{4}$$

with $\boldsymbol{V} = [\boldsymbol{v}_0\ -\boldsymbol{v}_1]$, $\boldsymbol{v}_i$, the view direction from the camera center corresponding to the tie feature i and t_i the position of the camera corresponding to the time at which tie feature i was seen by the camera based on the INS/GNSS trajectory and the initial value of system/camera intrinsics.

The *a-posteriori* uncertainty of the intrinsic parameters is computed using the methodology presented in (Cledat et al., 2020). Based on Laplace's approximation (MacKay, 2003), we know that the *a-posteriori* covariance of the parameters is approximately equal to the inverse of the Hessian from Equation 3:

$$\boldsymbol{\Sigma}_{\boldsymbol{x}\boldsymbol{x}} \approx \boldsymbol{H}^{-1}, \tag{5}$$

with equality when the functional model is linear and the stochastic model follows a normal distribution.

High *a-posteriori* uncertainties are indications that the parameters are weakly observable. On the other hand, large observation residuals indicates either a mismatch between the stochastic and functional models or occurrence of unexpected measurement errors. Since we use prior information for the camera intrinsic parameters derived from a lab calibration, a large residual is indicative of a measurement error.

The relative consistency of the estimated camera intrinsic parameters across multiple flights is obtained by comparing its variability across different missions together with their estimated *a-posteriori* uncertainties, or by using a multiple subset of the model to estimate the parameters multiple times, a process known as bootstrapping (Burkhard et al., 2024) (e.g., the boresight and lever arm of the camera can be recomputed from different flying lines to control the consistency of the estimated parameters).

3.2 Absolute accuracy

The absolute accuracy is subject to the availability of an external reference, which may represent a practical/logistic challenge, time and cost. In the case of geo-rectified imagery, an absolute reference is usually a ground control point or some other feature with known geographic coordinates. While some missions of AVIRIS-4 will be flown with the existence of such reference points, their presence cannot be assumed in general. Instead, we rely mostly on the initial SBET (separate INS/GNSS optimization), and the lab calibration of the camera intrinsic parameters as references to predict the absolute ground accuracy.

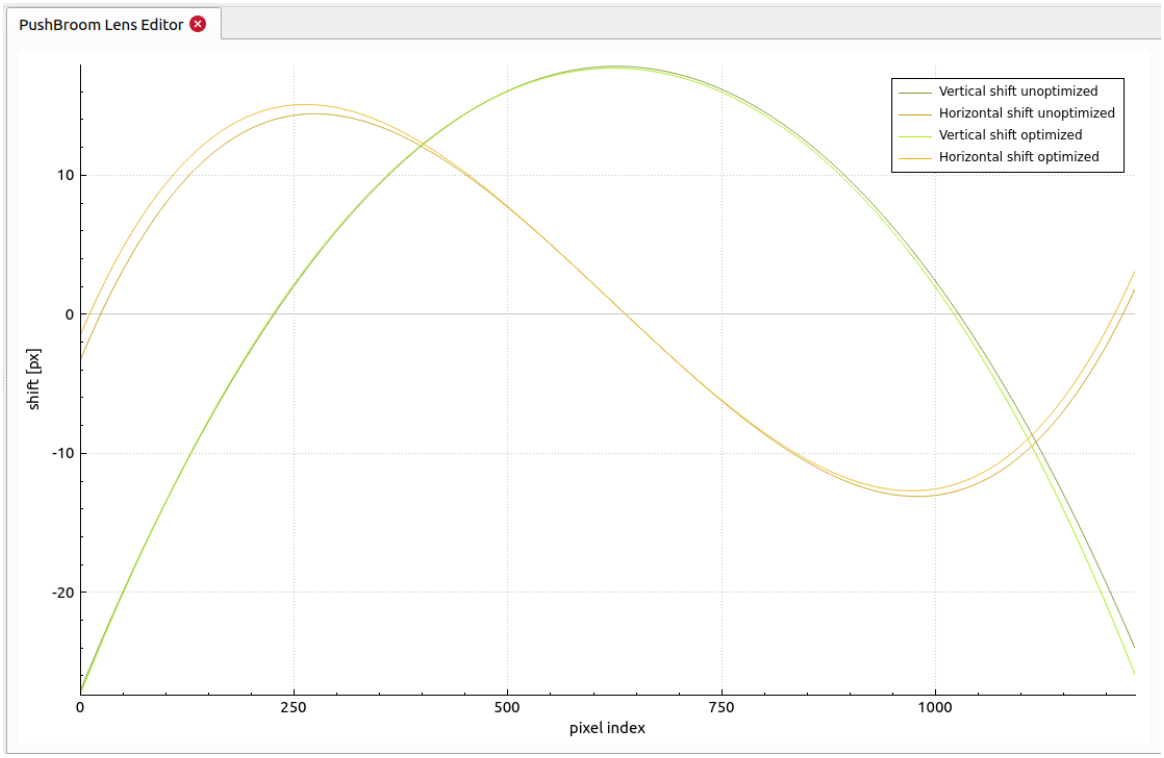

Figure 3. Push-broom lense distortion analysis in SteviApp, here with AVIRIS-4 optimized and laboratory calibrated lense distortion parameters. Legend: *horizontal* corresponds to *across-track* and *vertical* to *along-track* components.

The position residual of each camera-line $\Delta \boldsymbol{t}$ is computed for all three axis:

$$\Delta \boldsymbol{t} = \hat{\boldsymbol{t}} - \mathring{\boldsymbol{t}}, \tag{6}$$

with $\hat{\boldsymbol{t}}$ the position estimated after adjustment, and $\mathring{\boldsymbol{t}}$ the position prior

For the attitude, the residual $\Delta \boldsymbol{r}$ is measured on the $SO(3)$ manifold using differential geometry:

$$\Delta \boldsymbol{r} = log(\hat{\boldsymbol{R}}^{\top} \mathring{\boldsymbol{R}}), \tag{7}$$

where $\hat{\boldsymbol{R}}$ is the estimated orientation of the platform and $\mathring{\boldsymbol{R}}$ is the orientation from the initial SBET. The log-function here is the matrix logarithm, mapping from the space of rotation matrices to axis angles. For small angles the axis-angle can be interpreted as the error along each axis.

Concerning the camera-mount intrinsic parameters, the lever arm and boresight, Equation 6 and Equation 7 are used again, this time with the the mount values obtained separately (e.g. from AVIRIS-4 CAD plan for the camera-IMU lever-arm and zero or known Cardinal rotation for the boresight). As for the lens distortions, the fact that different parametrizations may represent the same distortion must be considered. As such, we recommend visual inspections of the resulting distortion curves via the viewing tool in SteviApp, as shown in Figure. 3. In practice, the calibrated lens distortion parameters will be kept constant across operational scientific mission flights without specific flight-line configurations intended for in-flight camera calibration.

4. Practical example

4.1 Test flights

We used two test flights in Swizerland: one performed over the city Zurich, where the AVIRIS-4 was mounted on an active stabilization device and two parallel lines were flown at the same height, over hilly terrain, and another over the city of Thun, consisting of four perpendicular flight lines, flown at different heights over (mostly) flat terrain. The active stabilization mount was configured in a locked configuration for part of the Thun flight lines, to improve the observability of the misalignment angles (bore-sight) between the inertial system and the AVIRIS-4 projective frame. The average ground sampling distance (GSD) of the data for both flights was approximately 0.4 meters. The flight path (along with the DSM) are shown in Figure 4. The navigation data was produced by an iXblue Atlans A7 navigation system attached to the spectrometer. In both cases, the INS data from the Atlans A7 were fused with differential GNSS processed position data using a Kalman Filter followed by recursive smoothing to produce an initial SBET. A total of 46 tie points were manually labeled for the Zurich flight and 314 landmarks were labeled for the Thun flight. DSM corresponding to the flight lines of each acquisition were obtained from the open source, airborne laser scanning swissSURFACE3D Raster data product provided by the Swiss Federal office of Topography.

4.2 Analysis

Trajectory residuals. In analyzing the data, we observe that, except for a few outliers, the trajectory residuals are negligible in position (to be expected for processed PPK-GNSS/INS) and non-negligible in attitude (0.06° or 0.001 radians), which is approximately one order of magnitude larger than the nominal accuracy of the iXBlue Atlans A7; see Figure 5. This indicates

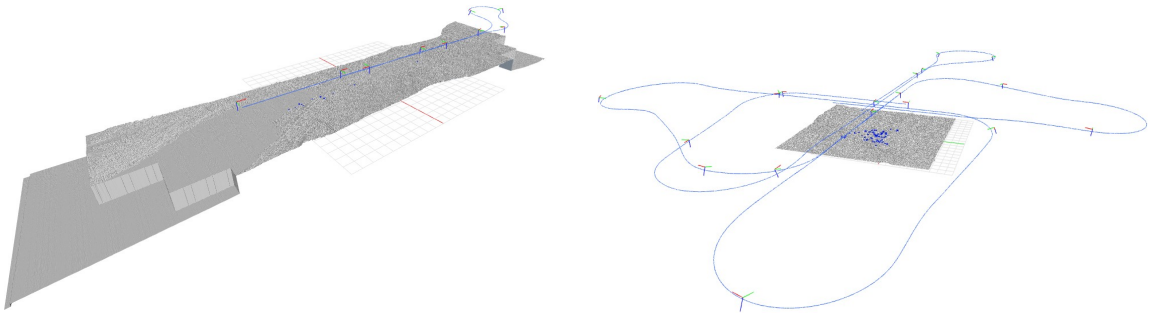

(a) Zurich (b) Thun

Figure 4. Two calibration flights under consideration (with their associated DSM to preview the terrain)

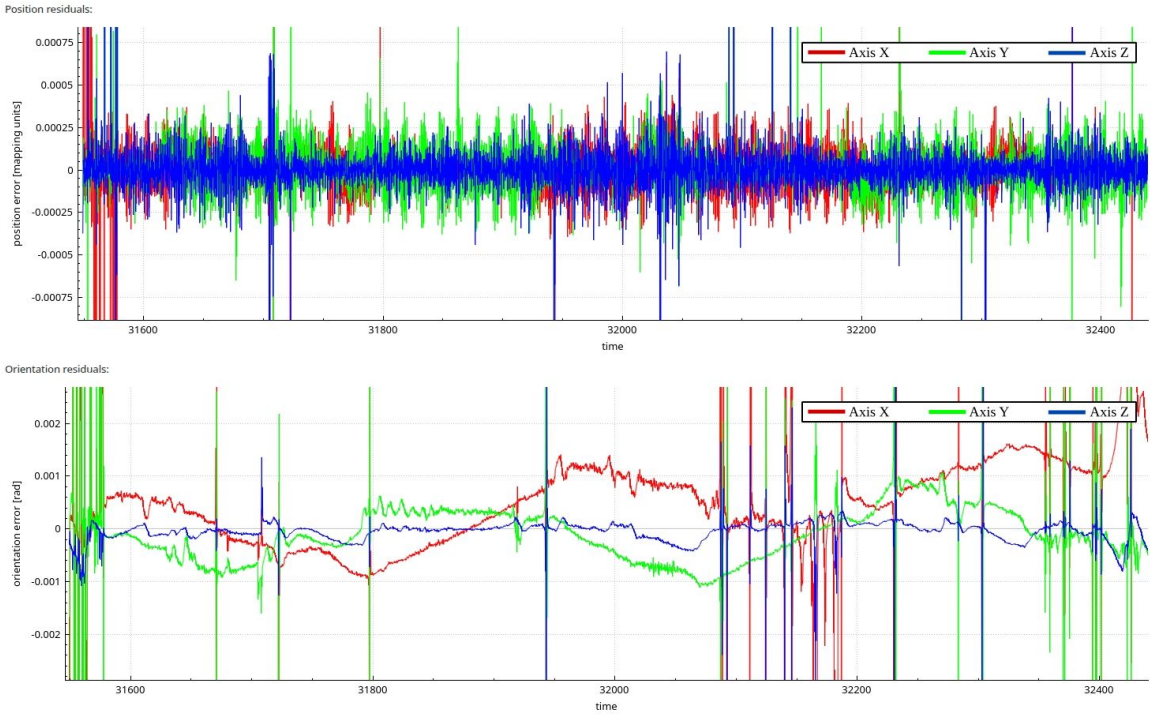

Figure 5. Trajectory residuals for Thun flight (in meters and radians)

that the optimized trajectory has errors in the estimated orientation which can be either due to unmodeled characteristics of the inertial sensors or the camera internal orientation, or both. The 0.06° orientation error represents an offset of approximately 3 pixels. To determine the root cause of the error, we reprocessed the raw navigation data (GNSS-INS) in three different software environments: (i) the recursive smoother of the iXblue inertial post-processing software, (ii) the optimal smoother of the Inertial Explorer software and (iii) the factor-graph based Dynamic Network (DN) (Cucci et al., 2017). All three resulting trajectories were consistent among themselves.

After further investigation it was found on the portion of flight where the mount stabilization was active, the recording of the mount-stabilization angles by Atlans A7 was incorrectly associated with the GPS time. This caused a bias in the estimated trajectory as the platform stabilization introduces a time-dependent projection of the distance between the IMU center and GNSS antenna on the IMU axes (variable lever-arm components). Ignoring the time variation in lever-arm components introduces error in the measured INS position which is propagated into the trajectory in the initial estimation and its subsequent optimization by SteviApp. The tie points labeled in SteviApp were later used to correct the Thun data prior to orthorectification and their subsequent analysis (Hueni et al., 2025). Work is ongoing to correct the hardware issue preventing the collection of correctly time-stamped angles during mount stabilization, so that they can be correctly accounted for in the sensor-fusion.

Tie-point reprojection. The manually identified tie-points and/or control-points by MALAHYD allow to performed reprojection error analysis. This helped to identify other issues, notably in the Zurich flight. The initial reprojection error for line 2 were significantly higher than for line 1. The root cause of the issue was a falsely recorded time-synchronization (PPS) message from the navigation system, which offset the time-tagging of the AIS sequence by 1 second. This significantly translated the georeferencing, mainly in the along-track direction on this image line. This is easy to identify by analysis of the reprojection errors between the two flight-lines, as shown in Figure 6. After correcting the time-stamping in the first line, the mean

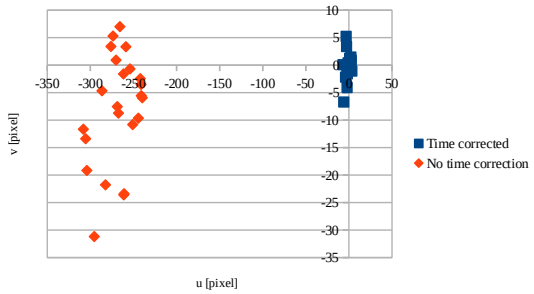

Figure 6. Reprojection error before and after time correction for Line 2 in the Zurich data

re-projection error depicted on Figure 7 for the Zurich data is approximately 3 pixels. This is about 3× higher than than the mean re-projection on Thun (approximately 1 pixel) shown in Figure 8. However, there seems to be a systematic effect for each line of 0.5-1 pixel. As a bias of 1px is +/- equivalent to a bias of 0.02° in attitude, this provides further evidence that there is a problem with the determination of the attitude when re-estimating the trajectory. The bias changes depending on the strip orientation, which suggests that it is due to inaccurate or unmodeled effects in the navigation system and unaccounted stabilization angles as discussed previously.

Boresight and lever arm. Estimation of the boresight between camera and IMU as well as the lever arm between camera and IMU and GPS is essential for precise georeferencing. Here we attempt to estimate just the IMU-camera elements, while taking the lever arm to GNSS antenna to the center of the mount as externally provided. The estimation of the camera center is consistent, both with the prior-information as well as between flights. Nevertheless, the the a-posteriori standard deviation remains high, indicating that this parameter is not clearly observable. In practice, the lever arm should be determined separately and better remain fixed during optimization. Nevertheless, for quality assurance it is useful to estimate it, as a lever arm vastly different from the prior is indicative of other issues (e.g. datum inconsistency of the trajectory and the provided DEM). In the case of the boresight, the small inconsistencies are likely due to the previously described issue in the attitude determination, albeit this indicator seems a bit inconclusive compared to the tie point reprojection plot.

5. Conclusion and outlook

We have presented an open utility for the manual labeling of hyperspectral images. This, so-named MALAHYD tool supports the efforts of ARES to provide open research data for the AVIRIS-4 sensor. We contribute towards these by providing a means to verify the accuracy of the final data, which enhances the interoperability of the data, in line with the FAIR principles.

Analysis of the first acquired AVIRIS-4 data has highlighted the utility of MALAHYD in the processing chain to identify errors that may otherwise be difficult to detect in direct orientation. Particularly, a time-tagging offset in the Zurich flight, recurrent problems in recording stabilization mount angles in the Thun flight, or an error in the DEM datum selection for the orthorectification.

At the time of writing, the MALAHYD and SteviApp tools are still under development, and will be so for the foreseeable future. Issues and help requests can be submitted to the github issue tracker.

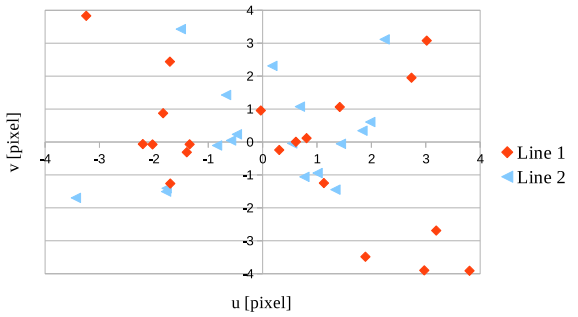

Figure 7. Reprojection error for Zurich lines (in pixels)

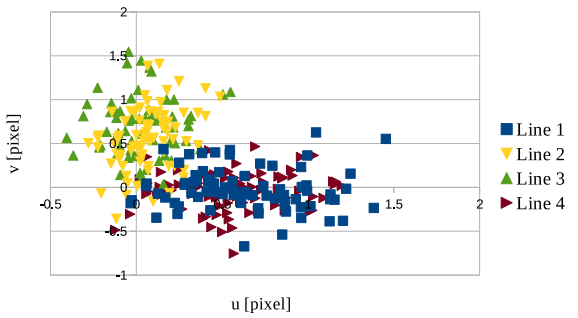

Figure 8. Reprojection error for Thun lines (in pixels)

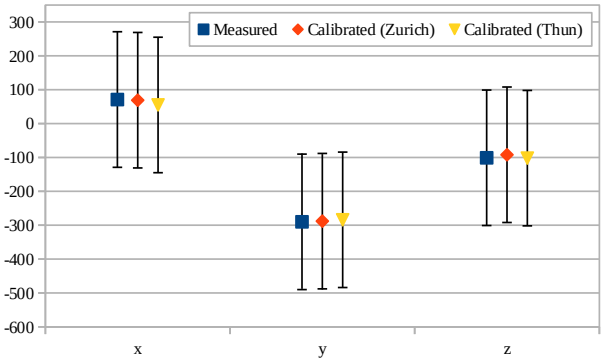

Figure 9. Measured and calibrated lever arm (in mm) for the AVIRIS-4 instrument with 1 σ deviation bars.

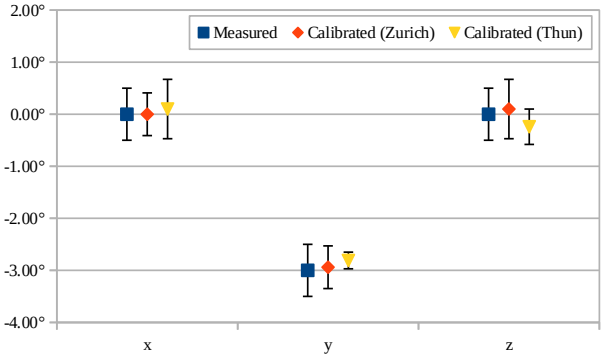

Figure 10. Measured and calibrated boresight (in °) for the AVIRIS-4 instrument with 1 σ deviation bars.

References

Behmann, J., Steinrücken, J., Plümer, L., 2014. Detection of early plant stress responses in hyperspectral images. *ISPRS Journal of Photogrammetry and Remote Sensing*, 93, 98–111.

Burkhard, J. Y., Lahaye, J. R. M., Jospin, L. V., Skaloud, J., 2024. In flight boresight rectification for lightweight airborne pushbroom imaging spectrometry.

Cledat, E., Jospin, L., Cucci, D., Skaloud, J., 2020. Mapping quality prediction for RTK/PPK-equipped micro-drones operating in complex natural environment. *ISPRS Journal of Photogrammetry and Remote Sensing*, 167, 24-38.

Cucci, D. A., Rehak, M., Skaloud, J., 2017. Bundle adjustment with raw inertial observations in UAV applications. *ISPRS Journal of Photogr. and Rem. Sens.*, 130, 1-12.

Hueni, A., Geier, S., Vögtli, M., LaHaye, J., Rosset, J., Berger, D., Sierro, L. J., Jospin, L. V., Thompson, D. R., Schläpfer, D., Green, R. O., Loeliger, T., Skaloud, J., Schaepman, M. E., 2025. The AVIRIS-4 Airborne Imaging Spectrometer. *Geoscience and Remote Sensing Letters*.

Jacobsen, A., de Miranda Azevedo, R., Juty, N., Batista, D., Coles, S., Cornet, R., Courtot, M., Crosas, M., Dumontier, M., Evelo, C. T. et al., 2020. Fair principles: interpretations and implementation considerations.

Jospin, L., 2023. Advances in Stereo Reconstruction towards Improved Holographic Communication. PhD thesis, The University of Western Australia.

Kumar, S., Torres, C., Ulutan, O., Ayasse, A., Roberts, D., Manjunath, B. S., 2020. Deep remote sensing methods for methane detection in overhead hyperspectral imagery. *Proceedings of the IEEE/CVF Winter Conference on Applications of Computer Vision (WACV)*.

MacKay, D. J., 2003. *Information theory, inference and learning algorithms*. Cambridge university press.

Schläpfer, D., Richter, R., 2002. Geo-atmospheric processing of airborne imaging spectrometry data. Part 1: Parametric orthorectification. *International Journal of Remote Sensing*, 23(13), 2609–2630.

Varade, D., Maurya, A. K., Sure, A., Dikshit, O., 2017. Supervised classification of snow cover using hyperspectral imagery. *2017 International Conference on Emerging Trends in Computing and Communication Technologies (ICETCCT)*, IEEE, 1–7.

Wilkinson, M. D., Dumontier, M., Aalbersberg, I. J., Appleton, G., Axton, M., Baak, A., Blomberg, N., Boiten, J.-W., da Silva Santos, L. B., Bourne, P. E., Bouwman, J., Brookes, A. J., Clark, T., Crosas, M., Dillo, I., Dumon, O., Edmunds, S., Evelo, C. T., Finkers, R., Gonzalez-Beltran, A., Gray, A. J., Groth, P., Goble, C., Grethe, J. S., Heringa, J., 't Hoen, P. A., Hooft, R., Kuhn, T., Kok, R., Kok, J., Lusher, S. J., Martone, M. E., Mons, A., Packer, A. L., Persson, B., Rocca-Serra, P., Roos, M., van Schaik, R., Sansone, S.-A., Schultes, E., Sengstag, T., Slater, T., Strawn, G., Swertz, M. A., Thompson, M., van der Lei, J., van Mulligen, E., Velterop, J., Waagmeester, A., Wittenburg, P., Wolstencroft, K., Zhao, J., Mons, B., 2016. The FAIR Guiding Principles for scientific data management and stewardship. *Scientific Data*, 3(1), 160018. https://doi.org/10.1038/sdata.2016.18.

Zhang, G., Xu, K., Zhang, Q., Li, D., 2018. Correction of Pushbroom Satellite Imagery Interior Distortions Independent of Ground Control Points. *Remote Sensing*, 10(1). https://www.mdpi.com/2072-4292/10/1/98.